



On the Production of Polyols and Hydroxycarboxylic Acids in Interstellar Analogous Ices of Methanol

Cheng Zhu^{1,2} , Andrew M. Turner^{1,2}, Cornelia Meinert³ , and Ralf I. Kaiser^{1,2} ¹Department of Chemistry, University of Hawaii at Mānoa, Honolulu, HI 96822, USA; ralfk@hawaii.edu²W.M. Keck Laboratory in Astrochemistry, University of Hawaii at Mānoa, Honolulu, HI 96822, USA³Université Côte d'Azur, Institut de Chimie de Nice, UMR 7272 CNRS, F-06108 Nice, France; Cornelia.Meinert@unice.fr

Received 2019 October 8; revised 2019 December 4; accepted 2019 December 12; published 2020 January 31

Abstract

This laboratory work studied the production of complex organic molecules in pure methanol (CH₃OH) ices exposed to ionizing radiation in the form of energetic electrons. The chemical evolution of the ices during the electron irradiation at 10 K and subsequent warm-up phase to 300 K was monitored online and in situ via Fourier Transform Infrared spectrometry. Polyols and hydroxycarboxylic acids related absorptions were observed in the infrared spectra of the irradiated ices and residues at room temperature. The residues were analyzed via two-dimensional gas chromatography coupled to time-of-flight mass spectrometry (GC × GC–TOFMS). Four polyols and five hydroxycarboxylic acids were detected. All of these compounds, except 1, 3-propanediol and 1, 3-butanediol, have been identified in the Murchison and Bell meteorites. The most abundant species, ethylene glycol, has also been found in the interstellar medium (ISM). Our findings suggest that other polyols and acids may also be present in methanol-rich star-forming regions. The non-detection of higher order sugars, such as those found in the ultraviolet photon-processed, ¹³C-methanol (¹³CH₃OH):water (H₂O):ammonia (NH₃), and ¹³CH₃OH: H₂O ice mixtures, indicates that the type of radiation source or more likely the prevalent NH₃ and/or H₂O molecules in the ISM are critical to the abiotic formation of the bio-essential sugars. Experiments are currently being designed to elucidate the roles of each component.

Unified Astronomy Thesaurus concepts: [Laboratory astrophysics \(2004\)](#); [Astrochemistry \(75\)](#); [Pre-biotic astrochemistry \(2079\)](#); [Meteorite composition \(1037\)](#); [Interstellar medium \(847\)](#)

1. Introduction

Over the last few decades, polyols (organic compounds containing multiple hydroxyl (-OH) groups) and hydroxycarboxylic acids (carboxylic acids (RCOOH) carrying one or more additional hydroxyl groups) have received substantial attention from the astronomy and laboratory astrochemistry communities due to their potential importance for astrobiology (Agarwal et al. 1985; Cooper et al. 2001; Hollis et al. 2002; Bennett et al. 2007; Nuevo et al. 2010; Maity et al. 2014, 2015; Nuevo & Sandford 2014; Kaiser et al. 2015; Meinert et al. 2016; Bergantini et al. 2017, 2018; Modica et al. 2018; Zhu et al. 2019). Ethylene glycol (HOCH₂CH₂OH), the simplest polyol, represents the only polyol detected in the gaseous interstellar medium (ISM) toward, e.g., Sagittarius B2(N-LMH) (Hollis et al. 2002) and the MM1 core in the high-mass star-forming region NGC 6334I (McGuire et al. 2017; Table 1). However, a rich spectrum of polyols and hydroxycarboxylic acids has been detected in the Murchison and Bell meteorites (Table 1; Cooper et al. 2001; Monroe & Pizzarello 2011; Cooper & Rios 2016). The presence of biologically related molecules, such as glycerol (HOCH₂CH(OH)CH₂OH) as a central precursor to lipids, and glyceric acid (HOCH₂CH(OH)COOH) being crucial in glycolysis in primitive meteorites, is consistent with the scenario that a significant amount of the organic compounds related to the biological processes on the early Earth might have been delivered by extraterrestrial objects to Earth (Oró 1961; Chyba & Sagan 1992).

In addition to searching for extraterrestrial sources, laboratory experiments exploiting ultraviolet (UV) light and energetic particles exposing interstellar analogous ice mixtures at low temperatures (10 to 80 K) have been performed in an attempt to simulate the formation of polyols and hydroxycarboxylic acids under astrophysical, non-biological conditions

(Table 1). Nevertheless, very often, these simulation experiments have been affected by contaminants. Agarwal et al. (1985) irradiated ice mixtures of carbon monoxide (CO)—ammonia (NH₃)—water (H₂O) with broad UV light at 10 K and tentatively identified ethylene glycol and glycerol in the residues. However, the authors admitted that these polyols are likely contaminants in the methanol used to extract the residues. In order to distinguish photochemical products from contaminants, irradiation experiments using isotopically labeled ices (¹³CO: ¹⁵NH₃:H₂¹⁸O) were conducted; these studies detected ethylene glycol (HOCH₂CH₂OH), glycerol (HOCH₂CH(OH)CH₂OH), glycolic acid (HOCH₂COOH), lactic acid (CH₃CH(OH)COOH), and 3-hydroxypropionic acid (HOCH₂CH₂COOH; Table 1; Briggs et al. 1992). Nonetheless, the experimental intensities of the labeled and unlabeled species are highly inconsistent with expected isotopic patterns making the results tentative. Materese et al. (2014) analyzed UV-irradiated nitrogen (N₂):¹³C-methane (¹³CH₄):¹³CO ices, but were only able to identify five acids (Table 1). Recent studies introduced methanol (CH₃OH) to ice mixtures (Nuevo et al. 2010; Meinert et al. 2016; Nuevo et al. 2018) as methanol is ubiquitous in the ISM at levels up to 30% of water in interstellar ices (Boogert et al. 2008; Bottinelli et al. 2010). Meinert et al. (2016) detected the most extensive polyols thus far: hydroxycarboxylic acids, and even ribose (HCO(CHOH)₄H) in the residues of photoprocessed H₂O:¹³CH₃OH:NH₃ ices. Since these studies used mixtures of ¹³CH₃OH with H₂O or H₂O and NH₃, it is challenging to reveal the role of each precursor in the reactions. Formose-type reactions, which do not involve ammonia, were proposed as the formation pathways of aldehydes and sugars (Shigemasa et al. 1977; Meinert et al. 2016), however, aldehydes—glycolaldehyde (HOCH₂CHO), lactaldehyde (CH₃CH(OH)CHO), and glyceraldehyde (HOCH₂CH(OH)CHO)—were not detected in the residues of photoprocessed H₂O:¹³CH₃OH ices, but

Table 1
Compilation of the Identified Polyols and Hydroxycarboxylic Acids ($\leq C_4$) in the Interstellar Medium (ISM), Meteorites, and Interstellar Analogous Ices

	Compound	Formula	Reference	
			ISM & Meteorite (1–5)	Interstellar Analog Ices(6–12)
Polyol	Ethylene glycol	HOCH ₂ CH ₂ OH	(1–3)	(6–8)
	1, 3-Propanediol	HOCH ₂ CH ₂ CH ₂ OH		(8, 10)
	Glycerol	HOCH ₂ CH(OH)CH ₂ OH	(3, 4)	(6–9, 11)
	Erythritol & Threitol	HOCH ₂ CH(OH)CH(OH)CH ₂ OH	(3, 4)	(8)
	2-Methyl glycerol	HOCH ₂ C(CH ₃)(OH)CH ₂ OH		(8)
	2-Hydroxymethyl glycerol	(HOCH ₂) ₂ C(OH)CH ₂ OH	(3)	(8)
Hydroxycarboxylic acid	Glycolic acid	HOCH ₂ COOH	(5)	(6–9, 12)
	Lactic acid	CH ₃ CH(OH)COOH	(5)	(6–8, 12)
	3-Hydroxypropionic acid	HOCH ₂ CH ₂ COOH	(5)	(7, 8, 12)
	Glyceric acid	HOCH ₂ CH(OH)COOH	(3, 4)	(6–9, 12)
	2-Hydroxybutyric acid	CH ₃ CH ₂ CH(OH)COOH	(5)	(8, 12)
	3-Hydroxybutyric acid	CH ₃ CH(OH)CH ₂ COOH	(5)	(8)
	4-Hydroxybutyric acid	HOCH ₂ CH ₂ CH ₂ COOH	(5)	(8)
	2-Hydroxymethyl glyceric acid	(HOCH ₂) ₂ C(OH)COOH	(3)	
	2-Hydroxyisobutyric acid	(CH ₃) ₂ C(OH)COOH	(5)	(8)
	2, 4-Dihydroxybutyric acid	HOCH ₂ CH ₂ CH(OH)COOH	(3, 4)	
	2, 3-Dihydroxybutyric acid & diastereomer	CH ₃ CH(OH)CH(OH)COOH	(3, 4)	
	3, 4-Dihydroxybutyric acid	HOCH ₂ CH(OH)CH ₂ COOH	(3, 4)	
	2-Methyl glyceric acid	HOCH ₂ C(CH ₃)(OH)COOH	(3, 4)	(8)
	Erythronic & Threonic acid	HOCH ₂ CH(OH)CH(OH)COOH	(3, 4)	(8)
	3-Hydroxyisobutyric acid	CH ₃ CH(CH ₂ OH)COOH	(5)	(8)
	Malic acid	HOCHCH ₂ CH(OH)COOH	(5)	(8)
	Tartaric & Mesotartaric acid	HOCHCH(OH)CH(OH)COOH	(4)	

References. (1) Hollis et al. (2002), (2) McGuire et al. (2017), (3) Cooper et al. (2001), (4) Cooper & Rios (2016), (5) Monroe & Pizzarello (2011), (6) Agarwal et al. (1985), (7) Briggs et al. (1992), (8) Meinert et al. (2016), (9) Nuevo et al. (2010), (10) Nuevo et al. (2018), (11) Kaiser et al. (2015), (12) Materese et al. (2014).

present in the experiments with the addition of ammonia (de Marcellus et al. 2015). These findings indicate that ammonia may participate in the formation of even nitrogen-free aldehydes and sugars and complicate the understanding of the detailed reaction mechanisms. Furthermore, the sources of oxygen (from ¹³CH₃OH or H₂O) in the detected products are unknown as well. Therefore, it is essential to perform experiments exploiting pure methanol first to examine its role in the formation of these complex organic molecules. Previous simulation experiments using pure methanol ices (Chen et al. 2013; Henderson & Gudipati 2015; Kaiser et al. 2015; Maity et al. 2015; Sullivan et al. 2016) confirmed simple polyols and hydroxycarboxylic acids, such as ethylene glycol (HOCH₂CH₂OH), glycerol (HOCH₂CH(OH)CH₂OH), and glycolic acid (HOCH₂COOH), during the temperature-programmed desorption (TPD) phase of UV light or energetic electrons processed ices.

Here, to rule out any contamination and to simplify the complexity of untangling possible reaction routes, we performed experiments of exposing pure CH₃OH as well as CH₃¹⁸OH ices to energetic electrons simulating cascades of secondary electrons generated by galactic cosmic-rays penetrating interstellar ices (Kaiser et al. 1997; Kaiser & Roessler 1997; Bennett et al. 2005) and analyzed the solid residues generated in the warm-up phase of the irradiated ices from 10 to 300 K. By using ¹⁸O substituted methanol, we reveal that ethylene glycol (HOCH₂CH₂OH), 1, 3-propanediol (HOCH₂CH₂CH₂OH), glycolic acid (HOCH₂COOH), 3-hydroxypropionic acid (HOCH₂CH₂COOH), 3-hydroxybutyric acid (CH₃CH(OH)CH₂COOH), 4-hydroxybutyric acid (HOCH₂CH₂CH₂COOH), glycerol (HOCH₂CH(OH)CH₂OH), and glyceric acid (HOCH₂CH(OH)COOH) can

be generated from the electron irradiation of pure methanol. Furthermore, we detected a new species, 1, 3-butenediol (HOCH₂CH₂CH(OH)CH₃), which has not been identified in previous laboratory residues. Methanol has been found to be ubiquitous in interstellar ices such as Orion BN and AFGL989 at levels of up to 30% with respect to water (Gibb et al. 2004). Since no laboratory simulation experiment can reproduce the chemical complexity and diverse radiation conditions of actual interstellar space simultaneously, we performed experiments using simple pure methanol ices first (Chen et al. 2013; Henderson & Gudipati 2015; Kaiser et al. 2015; Maity et al. 2015; Sullivan et al. 2016) before extending to more complex systems. Our experiments were conducted at doses of 168.9 ± 26.1 eV per methanol molecule representing typical life times of long-lived interstellar molecular clouds at ages of about 50 million years (Yeghikyan 2011; Jeffreson & Diederik Kruijssen 2018). No higher order sugars were found in the extractions of the residues, indicating that at least at doses below 168.9 ± 26.1 eV molecule⁻¹ water and/or ammonia may be critical for the formation of biologically relevant sugars detected in the residues of UV photon-processed H₂O:¹³CH₃OH:NH₃ and H₂O:¹³CH₃OH ices (de Marcellus et al. 2015; Meinert et al. 2016; Nuevo et al. 2018).

2. Experimental Methods

The experiments were carried out in a contamination-free ultrahigh vacuum chamber operating at a base pressure of 9×10^{-11} Torr (Zheng et al. 2006; Kaiser et al. 2013), which was achieved using two magnetically suspended turbo molecular

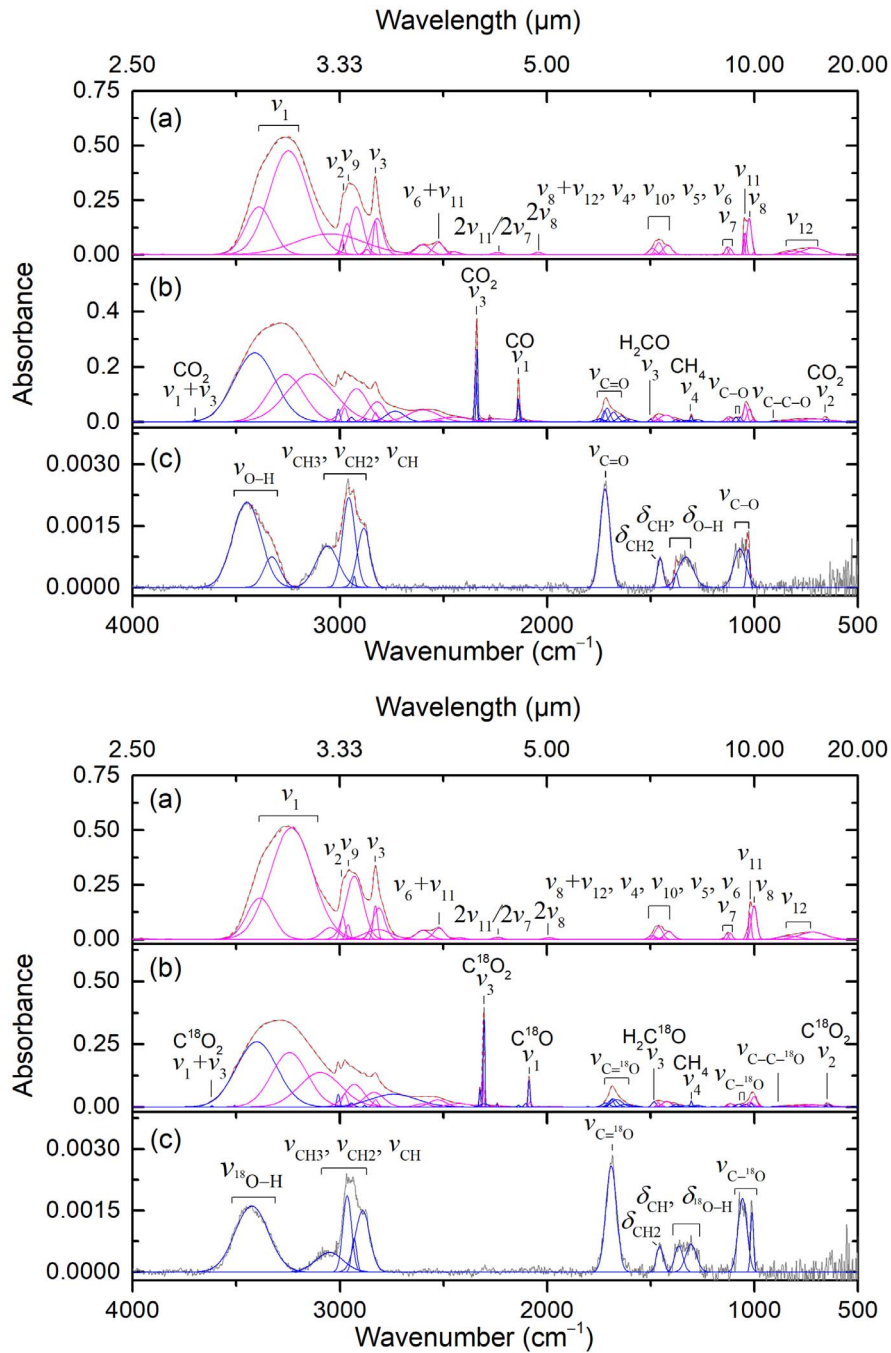


Figure 1. Deconvoluted infrared spectra of CH_3OH (top) and $\text{CH}_3^{18}\text{OH}$ (bottom) ices: (a) before the irradiation, (b) after the irradiation at 10 K, and (c) the residue at 300 K. Blue peaks represent absorptions induced by the irradiation. For clarity, only significant peaks are labeled; detailed assignments are compiled in Tables 3–5.

pumps (Osaka TG420 MCAB) coupled to two oil-free scroll pumps (Anest Iwata ISP-500). Within the chamber, a highly polished silver wafer was attached to an oxygen-free high-conductivity copper target and cooled by a two-stage closed cycle helium cryostat (CTI-Cryogenics 9600). After the wafer reached 10.0 ± 0.3 K, degassed methanol (CH_3OH ; Sigma Aldrich, 99.9%) or ^{18}O -methanol ($\text{CH}_3^{18}\text{OH}$; Sigma Aldrich, 95 atom% ^{18}O) was deposited on the substrate using a precision leak valve and glass capillary array at a pressure of 2×10^{-7} Torr in the main chamber for approximately 15 minutes. The ice growth was monitored in situ via laser interferometry with a helium–neon (He–Ne) laser (CVI Melles Griot; 25-LHP-230, 632.8 nm; Turner et al. 2015). The laser beam struck the silver wafer at an

angle of 2° relative to the ice surface normal and was reflected to a photodiode (CVI Melles Griot Silicon Photodiode; CVI XII-632.8–12.6 M) interfaced to a picoammeter (Keithley 6485). Considering the refractive index of methanol ice ($n_{\text{CH}_3\text{OH}} = 1.33 \pm 0.04$; Bouilloud et al. 2015), the ice thickness was calculated to be 900 ± 50 nm. The infrared spectra of the ices were recorded in a range of 6000 to 400 cm^{-1} with 4 cm^{-1} spectral resolution using a Nicolet 6700 Fourier Transform Infrared (FTIR) spectrometer (Figure 1(a)). With the absorption coefficients of 1.01×10^{-16} and 1.40×10^{-18} cm molecule^{-1} for the 3270 cm^{-1} (ν_1) and 1120 cm^{-1} (ν_{11}) bands (Bouilloud et al. 2015), respectively, the column density of methanol was found to be $(1.5 \pm 0.2) \times 10^{18}$ molecules cm^{-2} . Taking into account the

Table 2

Data Applied to Calculate the Average Irradiation Dose per Molecule

Initial kinetic energy of the electrons, E_{init} (keV)	5
Irradiation current, I (nA)	5000 ± 250
Total number of electrons	$(8.8 \pm 0.9) \times 10^{16}$
Average penetration depth, l (nm) ^a	420 ± 40
Maximum penetration depth, (nm) ^a	675 ± 70
Average kinetic energy of backscattered electrons, E_{bs} (keV) ^a	2.74 ± 0.27
Fraction of backscattered electrons, f_{bs} ^a	0.15 ± 0.02
Average kinetic energy of transmitted electrons, E_{trans} (keV) ^a	0
Fraction of transmitted electrons, f_{trans} ^a	0
Density of the ice, ρ (g cm ⁻³)	1.01 ± 0.03
Irradiated area, A (cm ²)	3.2 ± 0.3
Dose per methanol (eV molecule ⁻¹)	168.9 ± 26.1

Note.^a Parameters obtained from CASINO software v2.42.

density of methanol ($\rho_{\text{CH}_3\text{OH}} = 1.01 \pm 0.03$ g cm⁻³; Bouilloud et al. 2015), the ice thickness was calculated to be 800 ± 100 nm, which agrees well with the value determined using the laser interferometry method (900 ± 50 nm).

The ices were then irradiated isothermally at 10.0 ± 0.3 K with 5 keV electrons (Specs EQ 22–35 electron source) at a 15° angle relative to the target surface (3.2 ± 0.3 cm²) for 1 hour at a nominal current of 5000 nA with an extraction efficiency of the electrons of 78%. Exploiting Monte Carlo simulations (Casino 2.42; Drouin et al. 2007), the average and maximum penetration depths of the electrons were found to be 420 ± 40 nm and 675 ± 70 nm (Table 2), respectively, which is less than the ice thickness of 900 ± 50 nm ensuring no interaction between the electrons and the silver wafer. The average dose was calculated to be 168.9 ± 26.1 eV per methanol molecule. The irradiated ices were kept at 10.0 ± 0.3 K for one hour and then annealed at a rate of 1 K minutes⁻¹ to 300 K (TPD). During the irradiation and TPD phases, in situ FTIR spectra were recorded in intervals of 2 minutes (Figure 1, Tables 3–5).

After each experiment, the residue on the wafer was analyzed by a two-dimensional gas chromatographic (GC × GC) Pegasus IV D instrument coupled to a time-of-flight mass spectrometer (TOFMS; LECO, St. Joseph, Michigan, USA; Figure 2, Table 6). The TOFMS system operated at a storage rate of 150 Hz, with a mass range of 25–700 amu, a detector voltage of 1.6 kV, and a solvent delay of 10 minutes. The ion source and transfer temperatures were set to 503 K. The column set consists of an Agilent J&W DB 5MS Ultra Inert primary column (30 m × 0.25 mm inner diameter (ID), 0.25 μm film thickness) Press-Tight (Restek, Bellefonte, USA) connected to an Agilent DB Wax secondary column (1.40 m × 0.1 mm ID, 0.1 μm film thickness). The flow rate of carrier gas helium was used as carrier gas with a constant flow rate of 1 mL min⁻¹. Sample volumes of 1 μL were injected in the splitless mode into an ultra-inert, single taper splitless inlet liner with glass wool (Agilent) at an injector temperature of 503 K. All samples were studied with the same temperature program. The primary oven was controlled as follows: held 313 K for 1 minutes, warmed up to 463 K at a rate of 5 K min⁻¹ and held for 9 minutes. The secondary oven used the same temperature protocol with a constant temperature offset of 288 K except for the glycerol standard where a constant temperature offset of 303 K was used. The latter explains the

faster elution time of glycerol in the second dimension of the glycerol standard ($R_{t2} = 1.28$ s) compared to glycerol detected in all other injected samples ($R_{t2} = 1.40$ s, Table 6). A 5 s modulation period was applied for the liquid nitrogen cooled thermal modulator. Data were acquired and processed with LECO Corp ChromaTOF software. Compound identification was achieved by comparison with the chromatographic retention in both dimensions and mass spectra of authentic standards.

The derivatization reagents including trimethylsilyl chloride (TMCS) and *N, O*-bis(trimethylsilyl) trifluoroacetamide (BSTFA), the internal standard methyl laurate, and hexane as well as the reference standards of the polyols (ethylene glycol and glycerol), the saccharinic acid (glyceric acid), and the hydroxycarboxylic acids (glycolic, 3-hydroxypropionic, S-3-hydroxybutyric, and 4-hydroxybutyric) were purchased from Sigma Aldrich. Sample-handling glassware was wrapped in aluminum foil and heated at 773 K for 3 hr before usage to eliminate possible contamination. Eppendorf tips were sterile and the water exploited for extraction, standard solutions, reagent solutions, and blanks was of high-performance liquid chromatography grade. The residues were extracted with 6×50 μL water from their silver substrates and transferred into conical reaction vials (1 mL V-Vial, Wheaton). The aqueous extractions were dried under a gentle stream of nitrogen gas and silylated with an excess of 35 μL BSTFA and 5 μL TMCS for 2 hr at 353 K in the presence of the internal standard methyl laurate in hexane (5 μL, 10⁻⁵ M). The derivatized samples were transferred into GC vials for subsequent GC × GC–TOFMS analysis. Procedural blanks were run in sequence to each sample for monitoring significant background interferences. To eliminate any ¹⁶O contaminants, residues of the ¹⁸O-methanol (CH₃¹⁸OH) experiments were analyzed.

3. Results and Discussion

3.1. FTIR

Figure 1(b) depicts the FTIR spectra of the irradiated CH₃OH and CH₃¹⁸OH ices at 10.0 K. Table 4 compiles the assignments of the irradiation induced peaks. In addition to the decomposition of the precursor and formation of carbon dioxide (CO₂), carbon monoxide (CO), methane (CH₄), formaldehyde (H₂CO), and formyl radicals (HCO; Bennett et al. 2007; Maity et al. 2015), essential absorptions in the ranges of 1000–1100 cm⁻¹ ($\nu_{\text{C-O}}$), 1750–1700 cm⁻¹ ($\nu_{\text{C=O}}$), and 3600–3000 cm⁻¹ ($\nu_{\text{O-H}}$) were identified, which are related to functional groups of hydroxycarboxylic acids and/or polyols (Socrates 2004). These features are obscured by the precursor CH₃OH but remain in the residue at 300 K (Figure 1(c), Table 5). Experiments with CH₃¹⁸OH match the isotopic redshifts for the $\nu_{\text{C-O}}$ and $\nu_{\text{C=O}}$ modes by 20–30 cm⁻¹ (Friedel et al. 1967; Maity et al. 2015). These findings suggest that *functional groups* linked to hydroxycarboxylic acids and polyols can be generated by exposure of pure methanol ice to ionization radiation; however, functional groups are not unique to specific molecules due to the overlapping of the absorptions of homologous series and/or isomers (Socrates 2004). Therefore, the infrared analysis does not identify individual hydroxycarboxylic acid or polyol molecules.

3.2. GC × GC–TOFMS

To identify discrete molecular species, the residues were extracted, silylated, and analyzed via GC × GC–TOFMS (Figure 2 and Table 6). Compound identification was performed by comparison with the chromatographic retention in both

Table 3
Absorption Peaks Observed in Pristine CH₃OH and CH₃¹⁸OH Ices at 10 K^a

Wavenumber (cm ⁻¹)		Assignment
CH ₃ OH	CH ₃ ¹⁸ OH	
4396	4396	$\nu_2/\nu_9 + \nu_4/\nu_6/\nu_{10}$
4275	4275	$\nu_2/\nu_9 + \nu_4$
4095	4087	?
4012, 3983, 3954	3981, 3962, 3930	$\nu_2/\nu_9 + \nu_8$
3855	3828	?
3402, 3261, 3048	3386, 3233, 3047	ν_1
2989	2986	ν_2
2963	2960	ν_9
2920	2929	$\nu_4 + \nu_5/\nu_4 + \nu_{10}/\nu_5 + \nu_{10}/2\nu_4/2\nu_{10}/2\nu_5$
2872	2861	$2\nu_5/2\nu_{10}$
2828	2829	ν_3
2820	2813, 2811	$2\nu_6$
2600	2598	$\nu_4 + \nu_{11}/\nu_7 + \nu_4/\nu_6/\nu_{10}$
2525	2522	$\nu_6 + \nu_{11}$
2446	2423	$\nu_6 + \nu_8$
2239	2237	$2\nu_{11}/2\nu_7$
2042	1990	$2\nu_8$
1490	1491	$\nu_8 + \nu_{12}?$
1479	1478	ν_4
1460	1461	ν_{10}
1443	1443	ν_5
1418	1413	ν_6
1161, 1133, 1115	1157, 1132, 1115	ν_7
1049	1037,	ν_{11}
1042, 1024	1020, 1000	ν_8
1003	976	$\nu_8(^{13}\text{C})$
859, 805, 714	832, 718	ν_{12}

Note.

^a Assignments based on the references Bouilloud et al. (2015) and Maity et al. (2015).

dimensions of authentic standards and their corresponding mass spectra, as well as with previously reported data on trimethylsilyl (TMS) derivatives of polyols and hydroxycarboxylic acids (Meinert et al. 2016). Table 6 summarizes the retention times of analytes in the first and second chromatographic dimension as well as the corresponding mass spectra of the analyzed residue and standard. Figure 3 depicts the structures of the identified compounds in the residue. Four polyols and five hydroxycarboxylic acids were identified with an elution sequence of ethylene glycol, 1, 3-propanediol, glycolic acid, 1, 3-butanediol, 3-hydroxypropionic acid, 3-hydroxybutyric acid, 4-hydroxybutyric acid, glycerol, and glyceric acid. All of the following discussions about mass spectra are based on ¹⁸O substituted species. The mass spectra of all identified compounds are characterized by the intrinsic mass fragments of trimethyl silylated derivatives, i.e., by the absent molecular ion [M]⁺ peak, the fragment ion [M-15]⁺ formed by the loss of a methyl group from the (CH₃)₃Si-protecting group as well as silicon-containing fragments at $m/z = 45$ [CH₃SiH₂], 73 [(CH₃)₃Si], 75 [(CH₃)₃SiH₂], and 149 [(CH₃)₅Si¹⁸O]. Favored α -cleavage with charge retention followed by loss of trimethylsilyl group [(CH₃)₃Si-¹⁸OH] ($m/z = 92$) is observed as the predominant fragmentation pathway for all hydroxycarboxylic acids as well as polyols (McLafferty 1959; Gross 2004). Moreover, all hydroxycarboxylic acids undergo a McLafferty-type rearrangement (ester migration) of a (CH₃)₃Si group (McLafferty 1959; Gross 2004; Table 6). Glycerol and glyceric acid exhibit a common mass fragment of $m/z = 209$

[(CH₃)₃Si¹⁸OCH = CH¹⁸OSi (CH₃)₃]⁺, which is indicative of a vicinal diol group. Glyceric acid has a characteristic fragmentation pattern of stepwise loss of a methyl group (CH₃), a trimethylsilyl group [(CH₃)₃Si-¹⁸OH], and carbon monoxide (C¹⁸O) inducing the fragment of $m/z = 193$ [(CH₃)₂Si¹⁸OCH = CH¹⁸OSi(CH₃)₃]⁺ ([M-15-92-30]⁺) (Meinert et al. 2016).

3.3. Reaction Pathways

Having explicitly identified fully ¹⁸O substituted polyols and hydroxycarboxylic acids in the residues of irradiated and ¹⁸O-methanol (CH₃¹⁸OH) ices, we are now proposing possible formation pathways (Figure 4). Sophisticated infrared studies coupled with kinetics studies on the formation of small reaction intermediates and products reveal that upon exposure to energetic electrons at 10 K, methanol (CH₃OH) can decompose via atomic hydrogen loss leading to the methoxy (CH₃O; reaction (1)) and hydroxymethyl radicals (CH₂OH; reaction (2)); likewise, retro-insertion of electronically excited oxygen atoms (O(¹D)) forms methane (CH₄; reaction (3)); Bennett et al. 2007; Maity et al. 2014). Further, fragmentation of the methoxy (CH₃O) and hydroxymethyl radicals (CH₂OH) yields formaldehyde (H₂CO; reactions (4) and (5)), which then is eventually radiolyzed to carbon monoxide (CO) in one step through elimination of molecular hydrogen (reaction (6)) or via two steps involving the formyl (HCO) radical (reactions (7) and (8); Bennett et al. 2007). Then, atomic oxygen formed in reaction (3) may react with carbon monoxide generated via reaction (6)

Table 4
New Absorption Peaks Observed in CH₃OH and CH₃¹⁸OH Ices after the Irradiation at 10 K^a

Wavenumber (cm ⁻¹)		Assignment
CH ₃ OH	CH ₃ ¹⁸ OH	
3699	3618	CO ₂ ($\nu_1 + \nu_3$) ^b
...	3508	C ¹⁸ O ₂ ($2\nu_2 + \nu_3$)
3410	3401	O–H stretch ^b
3007, 2942, 2881, 2733	3008, 2944, 2880, 2740	CH ₃ , CH ₂ , and CH stretch (Aliphatic)
2345, 2339	2342	CO ₂ (ν_3)
...	2325	OC ¹⁸ O (ν_3)
...	2305, 2304	C ¹⁸ O ₂ (ν_3)
...	2240	¹³ C ¹⁸ O ₂ (ν_3)
2276	...	¹³ CO ₂ (ν_3)
2138, 2136	2137	CO (ν_1)
...	2087	C ¹⁸ O (ν_1)
1844	1802	HCO (ν_3) ^b
1744, 1722, 1708, 1678, 1641	1715, 1686, 1681, 1661, 1622	C=O stretch ^b
1499	1483	H ₂ CO(ν_3) ^b
1376, 1352, 1330	1378, 1351, 1338	CH bending and OH bending ^b
1304, 1303	1303	CH ₄ (ν_4)
1270, 1213, 1199	1273, 1189	CH ₂ twisting and OH bending ^b
1089, 1066	1074, 1043, 1014	C–O stretch ^b
917, 895	904, 868	C–C–O stretch ^b
663, 653	653, 344	CO ₂ (ν_2) ^b

Notes.

^a Assignments based on the references Bouilloud et al. (2015), Maity et al. (2015), and Socrates (2004).

^b For the CH₃¹⁸OH ice, oxygen atoms are ¹⁸O substituted.

Table 5
Absorption Peaks Observed in the Residues of Irradiated CH₃OH and CH₃¹⁸OH Ices at 300 K^a

Wavenumber (cm ⁻¹)		Assignment
CH ₃ OH	CH ₃ ¹⁸ OH	
3449, 3328, 3061	3245, 3051	O–H stretch ^b
2957, 2931, 2885	2964, 2931, 2890	CH ₃ , CH ₂ , and CH stretch (Aliphatic)
1721	1691	C=O stretch ^b
1454	1456	CH ₂ scissoring
1373, 1325	1375, 1316	CH bending and OH bending ^b
1070, 1031	1058, 1012	C–O stretch ^b

Notes.

^a Assignments based on the reference Socrates (2004).

^b For the CH₃¹⁸OH ice, oxygen atoms are ¹⁸O substituted.

to yield carbon dioxide (CO₂; reaction (9); Bennett et al. 2004, 2009a, 2009b). Therefore, the initial decomposition and radiolysis forms primary (CH₃O, CH₂OH, CH₄) and higher order products, e.g., carbon dioxide (CO₂; Bennett et al. 2007).

The hydroxymethyl radical (CH₂OH) has been shown to recombine with a second hydroxymethyl radical (CH₂OH) barrierlessly leading to the formation of ethylene glycol (reaction (10); Figure 4; Butscher et al. 2015; Zhu et al. 2019). Likewise, the hydroxycarbonyl radical (HOCO)—generated via reaction of suprathermal hydrogen atoms with carbon dioxide (reaction (11))—can react with carbon-centered radicals also barrierlessly (Bennett & Kaiser 2007; Kim & Kaiser 2010; Zhu et al. 2018); here, the hydroxycarbonyl radical (HOCO) may react with the hydroxymethyl radical (CH₂OH) to yield glycolic acid (reaction (12)). Further, the hydroxymethyl radical (CH₂OH) can recombine also without barrier with a methyl radical (CH₃) generated via

hydrogen loss from methane (reaction (13); Bennett et al. 2006; He et al. 2010; Jones & Kaiser 2013; Abplanalp et al. 2018) to ethanol (CH₃CH₂OH) (reaction (14); Bergantini et al. 2018). Note that ethanol was not detected in room-temperature residues since this molecule sublimates quantitatively between 130 and 150 K as the irradiated ice is warmed up to 300 K (Öberg et al. 2009; Abou Mrad et al. 2016; Bergantini et al. 2017, 2018). These products (ethylene glycol, glycolic acid, ethanol) represent critical building blocks in the molecular mass growth to higher order polyols and hydroxycarboxylic acids.

Radiolysis of ethylene glycol, glycolic acid, and ethanol followed by reactions with key primary (CH₂OH, CH₄) and higher order (CO₂) species can synthesize three-carbon-containing species: glycerol, glyceric acid, 3-hydroxypropionic acid, 1-propanol, and 1, 3-propanediol (reactions (15) to (22)). In detail, radiolysis of ethylene glycol via hydrogen atom loss forms the 1, 2-dihydroxyethyl radical (HOCH₂CHOH; reaction (15)), which then recombines with a hydroxymethyl radical (CH₂OH) to glycerol (reaction (16); Kaiser et al. 2015; Fedoseev et al. 2017). The methyl-carboxyhydroxy radical (HOCHCOOH; Leroy et al. 1991)—generated via decomposition of glycolic acid (reaction (17))—can react with a hydroxymethyl radical (CH₂OH) forming glyceric acid (reaction (18)). Radiolysis of ethanol produces 2-hydroxyethyl radical (CH₂CH₂OH; reaction (19)), which can recombine with hydroxycarbonyl (HOCO), methyl (CH₃), and hydroxymethyl (CH₂OH) radicals generating 3-hydroxypropionic acid (reaction (20)), 1-propanol (reaction (21)), and 1, 3-propanediol (reaction (22)), respectively.

Four-carbon-containing species can be generated in similar radical–radical recombination reactions. In detail, electron irradiation of 3-hydroxypropionic acid, 1-propanol, and 1, 3-propanediol can generate ethyl-2-carboxy-1-hydroxy (HOCHCH₂COOH; reaction (23)), 3-hydroxypropyl (CH₂CH₂CH₂OH; Ferro-Costas et al. 2018; reaction (24)), and propyl-1, 3-dihydroxy (HOCH₂CH₂

Table 6
Identified Compounds as Trimethylsilyl (TMS) Derivatives in Interstellar Analog Ices Initially Composed of $\text{CH}_3^{18}\text{OH}$ by GC \times GC-TOFMS

Compound	R_{t1} ^a (min)	R_{t2} ^b (s)	MS-fragmentation/ ¹⁸ O sample		MS-fragmentation/O reference standard		Relative amount (%) ^f
			[M ⁺] ^c	Other important ions, m/z	[M ⁺] ^c	Other important ions, m/z	
Ethylene glycol	11.15	1.42	<i>210</i>	195, 149, 105, 73	206	191, 147, 103, 73	100.00
1, 3-Propanediol	13.20	1.41	224	209, 181, 149, 132, 117, 73	220	205, 177, 147, 130, 115, 73	9.86 \pm 0.99
Glycolic acid	13.55	1.78	226	211, 181 ^d , 163, 149, 105, 73	220	205, 177 ^d , 161, 147, 103, 73	19.58 \pm 1.96
1, 3-Butanediol ^e	13.60	1.37	238	223, 149, 131, 119, 105, 73	234	219, 147, 129, 117, 103, 73	5.21 \pm 0.52
3-Hydroxypropionic acid	15.40	1.78	240	225, 181 ^d , 149, 118, 103, 73	234	219, 177 ^d , 147, 116, 101, 73	13.41 \pm 1.34
3-Hydroxybutyric acid	16.05	1.63	254	239, 195 ^d , 149, 119, 73	248	233, 191 ^d , 147, 117, 73	4.83 \pm 0.48
4-Hydroxybutyric acid	18.10	1.78	254	239, 208 ^d , 149, 119, 73	248	233, 204 ^d , 147, 117, 73	0.93 \pm 0.10
Glycerol	19.10	1.40	314	299, 222, 209, 149, 121, 105, 73	308	293, 218, 205, 147, 117, 103, 73	14.67 \pm 1.47
Glyceric acid	20.35	1.58	330	298 ^d , 209, 193, 179, 149, 121, 73	322	292 ^d , 205, 189, 175, 147, 117, 73	1.85 \pm 0.18

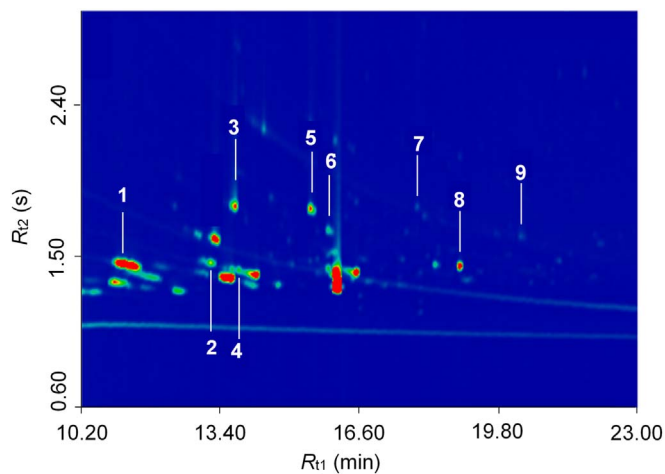
Notes.^a GC \times GC retention time 1st dimension.^b GC \times GC retention time 2nd dimension.^c Molecular ion peak *in italics* not detected.^d McLafferty-type (ester migration) rearrangement.^e Has not been detected in previous laboratory residues.^f Relative amount with respect to ethylene glycol.

Figure 2. GC \times GC-TOFMS chromatogram of the solvated residues of the irradiated $\text{CH}_3^{18}\text{OH}$ ices. Identified compounds include: (1) ethylene glycol, (2) 1, 3-propanediol, (3) glycolic acid, (4) 1, 3-butanediol, (5) 3-hydroxypropionic acid, (6) 3-hydroxybutyric acid, (7) 4-hydroxybutyric acid, (8) glycerol, and (9) glyceric acid.

CHOH; Buley et al. 1966; reaction (25)) radicals, which then recombine with methyl (CH_3), hydroxycarbonyl (HOCO), and methyl (CH_3) radicals producing 3-hydroxybutyric acid (reaction (26)), 4-hydroxybutyric acid (reaction (27)), and 1, 3-butanediol (reaction (28)), respectively.

Quantification of the detected molecules supports the proposed “bottom up” reaction pathways involving stepwise mass growth processes. As shown in Table 6, the sequences of the relative amount of each species with respect to ethylene glycol are found to be ethylene glycol (100.00%) > glycerol ((14.67 \pm 1.47)%), glycolic acid ((19.58 \pm 1.93)% > glyceric acid ((1.85 \pm 0.18)%), 3-hydroxypropionic acid ((13.41 \pm 1.34)% > 3-hydroxybutyric acid ((4.83 \pm 0.48)%), and 1, 3-propanediol ((9.86 \pm 0.99)% > 1, 3-butanediol ((5.21 \pm 0.52)%). These results are consistent with the proposal that glycerol, glyceric acid, 3-hydroxybutyric acid, and 1,

3-butanediol are secondary products of ethylene glycol, glycolic acid, 3-hydroxypropionic acid, and 1, 3-propanediol, respectively (Figure 4). Previous analysis of the volatile organic compounds released during a warming-up phase of a photoprocessed methanol ice also found that the abundances of C2 to C4 compounds decrease with the increase of their carbon chain length (Abou Mrad et al. 2016). Note that since the identified products were generated in solid-phase, numerous primary and secondary reactions might be coupled. Deciphering all possible elementary reactions is infeasible and out of the scope of this study. The identified molecules may also be generated in the TPD phase.

4. Astrophysical Implications

In the present study, we observe the formation of four polyols: ethylene glycol ($\text{HOCH}_2\text{CH}_2\text{OH}$), 1, 3-propanediol ($\text{HOCH}_2\text{CH}_2\text{CH}_2\text{OH}$), glycerol ($\text{HOCH}_2\text{CH}(\text{OH})\text{CH}_2\text{OH}$), and 1, 3-butanediol ($\text{HOCH}_2\text{CH}_2\text{CH}(\text{OH})\text{CH}_3$), and five hydroxycarboxylic acids: glycolic acid (HOCH_2COOH), glyceric acid ($\text{HOCH}_2\text{CH}(\text{OH})\text{COOH}$), 3-hydroxypropionic acid ($\text{HOCH}_2\text{CH}_2\text{COOH}$), 3-hydroxybutyric acid ($\text{CH}_3\text{CH}(\text{OH})\text{CH}_2\text{COOH}$), and 4-hydroxybutyric acid ($\text{HOCH}_2\text{CH}_2\text{CH}_2\text{COOH}$), in methanol ices upon interaction with ionizing radiation at 10 K, at radiation doses equivalent to those interstellar ices received during the lifetime of long-lived molecular clouds of about few 10^7 yr. These molecules were detected in the extractions of the room-temperature residues of the irradiated ^{18}O -methanol ($\text{CH}_3^{18}\text{OH}$) ice using GC \times GC-TOFMS. Since our derivatization reagents do not react with aldehydes (no -OH group), these species, such as formaldehyde (H_2CO), acetaldehyde (CH_3CHO), glyoxal (OCHCHO), and methylglyoxal (CH_3COCHO), were not detected in the residues. All detected polyols and hydroxycarboxylic acids except 1, 3-propanediol and 1, 3-butanediol have been identified in the Murchison and Bell meteorites (Cooper et al. 2001; Monroe & Pizzarello 2011; Cooper & Rios 2016). Among these compounds, the most abundant one, ethylene glycol, has been detected in methanol-rich comets, such as C/1995 O1 (Hale-Bopp; Crovisier et al. 2004)

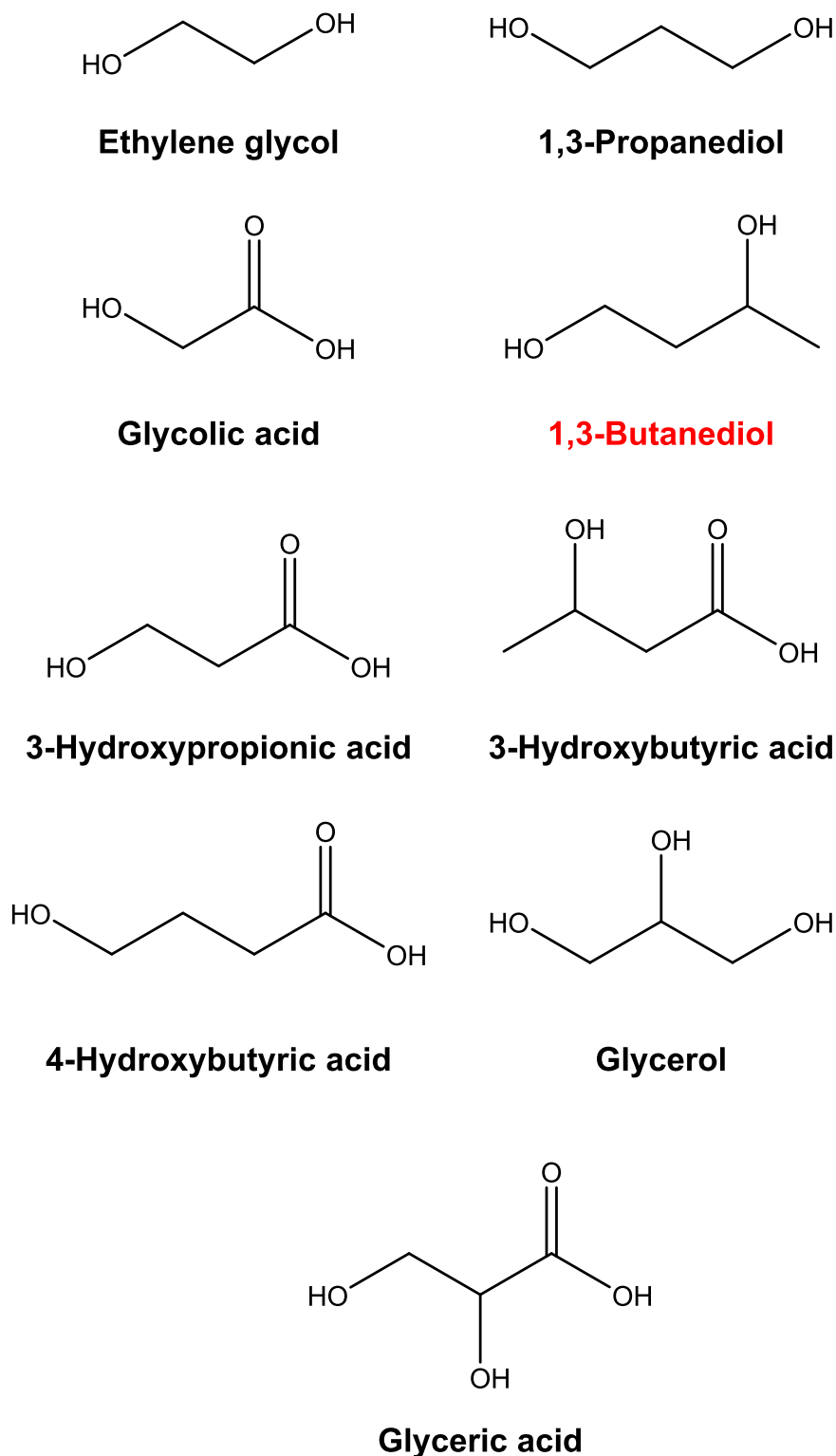


Figure 3. Molecular structures of ^{18}O labeled compounds in irradiated $\text{CH}_3^{18}\text{OH}$ ices by GC \times GC-TOFMS. 1, 3-Butanediol- ^{18}O is a new species that has not been reported in previous laboratory studies.

and 67P/Churyumov–Gerasimenko (Altwegg et al. 2017; Schuhmann et al. 2019). The double focusing mass spectrometer of the *Rosetta* Orbiter Spectrometer for Ion and Neutral Analysis instrument suite onboard the *Rosetta* Spacecraft detected signals at $m/z = 92$, which could be linked to glycerol (Altwegg et al. 2017). However, major fragments of glycerol are missing indicating that the peak at $m/z = 92$ may be mainly contributed

by toluene (C_7H_8 ; Schuhmann et al. 2019). Ethylene glycol has also been found in the ISM (Hollis et al. 2002; McGuire et al. 2017). Our findings suggest that methanol-rich star-forming regions are probably good candidates for future astronomical searches for these molecules, especially the central backbone of lipids—glycerol—since its formation efficiency is second only to ethylene glycol.

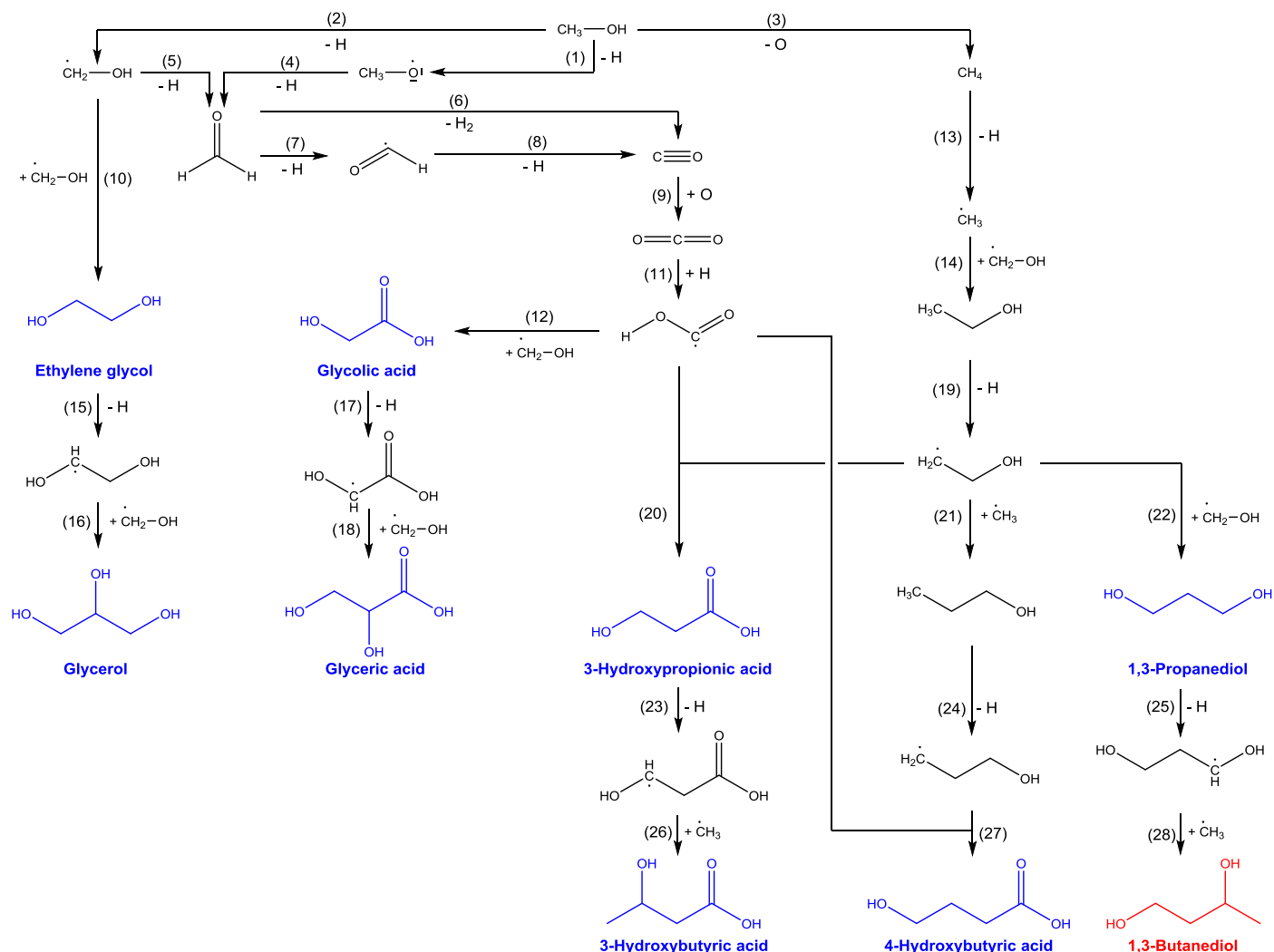


Figure 4. Proposed formation pathways of the detected polyols and hydroxycarboxylic acids. Species in blue and red are identified in irradiated $\text{CH}_3^{18}\text{OH}$ ices by GC \times GC-TOFMS. The one in red has not been reported in previous laboratory studies.

Note that no higher order sugars were detected in our residues. However, previous studies found extensive sugars from C_3 to C_5 , including the essential component of ribonucleic acid and adenosine triphosphate—ribose ($\text{HCO}(\text{CHOH})_4\text{H}$), in the residues of UV light irradiated $^{13}\text{CH}_3\text{OH}:\text{NH}_3:\text{H}_2\text{O}$ ice mixtures (Meinert et al. 2016). Exposure of $^{13}\text{CH}_3\text{OH}:\text{H}_2\text{O}$ ices to UV-radiation generated the sugar of DNA, 2-deoxyribose (Nuevo et al. 2018). The differences between the present work and previous studies are radiation sources (energetic electrons versus UV photons), energy doses, and ice compositions ($\text{CH}_3^{18}\text{OH}$ versus $^{13}\text{CH}_3\text{OH}:\text{NH}_3:\text{H}_2\text{O}$ and $^{13}\text{CH}_3\text{OH}:\text{H}_2\text{O}$). Previous studies have investigated the effects of each precursor on products properties (Bernstein et al. 1995; Muñoz Caro & Schutte 2003; Nuevo et al. 2011; Henderson & Gudipati 2015; Abou Mrad et al. 2017; Fresneau et al. 2017). Methanol was found to be the most reactive species and the main source of oxygen in products (Bernstein et al. 1995; Henderson & Gudipati 2015; Fresneau et al. 2017). The fraction of ammonia in the precursors does not alter the O/C ratio of the products significantly (Fresneau et al. 2017). An excess of H_2O can increase the abundance of more complex molecules due to molecular trapping effects (Fresneau et al. 2017), which may explain why high order sugars are missing in this study as our precursor is only pure methanol. We do not rule out the

possibility of more complex sugars in our residues but out of detection limit since the generation efficiency decreases upon increasing of molecular complexity (Abou Mrad et al. 2016). Future experiments by exposing $\text{CH}_3^{18}\text{OH}:\text{H}_2\text{O}$ and $\text{CH}_3^{18}\text{OH}:\text{NH}_3:\text{H}_2\text{O}$ ice mixtures to energetic electrons are planned to investigate if the type of radiation source or the prevalent NH_3 and H_2O molecules in the ISM (Mottl et al. 2007), or both, play critical roles in the abiotic formation of bio-essential sugars.

The Hawaii group acknowledges support from the US National Science Foundation, Division of Astronomical Sciences under grant AST-1800975. C. M. received funding by the French government through the UCAJEDI Investments in the Future Project managed by the National Research Agency (ANR) with the reference number ANR-15-IDEX-01 and the European Research Council under the European Union’s Horizon 2020 research and innovation program (grant agreement 804144).

ORCID iDs

Cheng Zhu <https://orcid.org/0000-0002-7256-672X>
 Cornelia Meinert <https://orcid.org/0000-0002-7256-2112>
 Ralf I. Kaiser <https://orcid.org/0000-0002-7233-7206>

References

- Abou Mrad, N., Duvernay, F., Chiavassa, T., & Danger, G. 2016, *MNRAS*, **458**, 1234
- Abou Mrad, N., Duvernay, F., Isnard, R., Chiavassa, T., & Danger, G. 2017, *ApJ*, **846**, 124
- Abplanalp, M. J., Jones, B. M., & Kaiser, R. I. 2018, *PCCP*, **20**, 5435
- Agarwal, V. K., Schutte, W., Greenberg, J. M., et al. 1985, *OrLj*, **16**, 21
- Altwegg, K., Balsiger, H., Berthelier, J.-J., et al. 2017, *MNRAS*, **469**, S130
- Bennett, C. J., Chen, S.-H., Sun, B.-J., Chang, A. H., & Kaiser, R. I. 2007, *ApJ*, **660**, 1588
- Bennett, C. J., Jamieson, C., Mebel, A. M., & Kaiser, R. I. 2004, *PCCP*, **6**, 735
- Bennett, C. J., Jamieson, C. S., & Kaiser, R. I. 2009a, *ApJS*, **182**, 1
- Bennett, C. J., Jamieson, C. S., & Kaiser, R. I. 2009b, *PCCP*, **11**, 4210
- Bennett, C. J., Jamieson, C. S., Osamura, Y., & Kaiser, R. I. 2006, *ApJ*, **653**, 792
- Bennett, C. J., & Kaiser, R. I. 2007, *ApJ*, **660**, 1289
- Bennett, C. J., Osamura, Y., Lebar, M. D., & Kaiser, R. I. 2005, *ApJ*, **634**, 698
- Bergantini, A., Góbi, S., Abplanalp, M. J., & Kaiser, R. I. 2018, *ApJ*, **852**, 70
- Bergantini, A., Maksyutenko, P., & Kaiser, R. I. 2017, *ApJ*, **841**, 96
- Bernstein, M. P., Sandford, S. A., Allamandola, L. J., Chang, S., & Scharberg, M. A. 1995, *ApJ*, **454**, 327
- Boogert, A. C. A., Pontoppidan, K. M., Knez, C., et al. 2008, *ApJ*, **678**, 985
- Bottinelli, S., Boogert, A. C. A., Bouwman, J., et al. 2010, *ApJ*, **718**, 1100
- Bouilloud, M., Fray, N., Benilan, Y., et al. 2015, *MNRAS*, **451**, 2145
- Briggs, R., Ertem, G., Ferris, J. P., et al. 1992, *OLEB*, **22**, 287
- Buley, A. L., Norman, R. O. C., & Pritchett, R. J. 1966, *JCSBPO*, **0**, 849
- Butscher, T., Duvernay, F., Theule, P., et al. 2015, *MNRAS*, **453**, 1587
- Chen, Y.-J., Ciaravella, A., Muñoz Caro, G. M., et al. 2013, *ApJ*, **778**, 162
- Chyba, C., & Sagan, C. 1992, *Natur*, **355**, 125
- Cooper, G., Kimmich, N., Belisle, W., et al. 2001, *Natur*, **414**, 879
- Cooper, G., & Rios, A. C. 2016, *PNAS*, **113**, E3322
- Crovisier, J., Bockelée-Morvan, D., Biver, N., et al. 2004, *A&A*, **418**, L35
- de Marcellus, P., Meinert, C., Myrgorodska, I., et al. 2015, *PNAS*, **112**, 965
- Drouin, D., Couture, A. R., Joly, D., et al. 2007, *Scanning*, **29**, 92
- Fedoseev, G., Chuang, K.-J., Ioppolo, S., et al. 2017, *ApJ*, **842**, 52
- Ferro-Costas, D., Martínez-Núñez, E., Rodríguez-Otero, J., et al. 2018, *JPCA*, **122**, 4790
- Fresneau, A., Abou Mrad, N., d'Hendecourt, L. L., et al. 2017, *ApJ*, **837**, 168
- Friedel, R. A., Durie, R. A., & Shewchuk, Y. 1967, *Carbon*, **5**, 559
- Gibb, E. L., Whittet, D. C. B., Boogert, A. C. A., & Tielens, A. G. G. M. 2004, *ApJS*, **151**, 35
- Gross, J. H. 2004, *Mass Spectrometry-A Textbook* (Heidelberg: Springer)
- He, J., Gao, K., Vidali, G., Bennett, C. J., & Kaiser, R. I. 2010, *ApJ*, **721**, 1656
- Henderson, B. L., & Gudipati, M. S. 2015, *ApJ*, **800**, 66
- Hollis, J. M., Lovas, F. J., Jewell, P. R., & Coudert, L. 2002, *ApJL*, **571**, L59
- Jeffreson, S. M. R., & Diederik Kruijssen, J. M. 2018, *MNRAS*, **476**, 3688
- Jones, B. M., & Kaiser, R. I. 2013, *JPCL*, **4**, 1965
- Kaiser, R. I., Eich, G., Gabrysch, A., & Roessler, K. 1997, *ApJ*, **484**, 487
- Kaiser, R. I., Maity, S., & Jones, B. M. 2015, *AChIE*, **54**, 195
- Kaiser, R. I., & Roessler, K. 1997, *ApJ*, **475**, 144
- Kaiser, R. I., Stockton, A. M., Kim, Y. S., Jensen, E. C., & Mathies, R. A. 2013, *ApJ*, **765**, 111
- Kim, Y. S., & Kaiser, R. I. 2010, *ApJ*, **725**, 1002
- Leroy, G., Sana, M., & Wilante, C. 1991, *JMoStT*, **247**, 199
- Maity, S., Kaiser, R. I., & Jones, B. M. 2014, *FaDi*, **168**, 485
- Maity, S., Kaiser, R. I., & Jones, B. M. 2015, *PCCP*, **17**, 3081
- Materese, C. K., Cruikshank, D. P., Sandford, S. A., et al. 2014, *ApJ*, **788**, 111
- McGuire, B. A., Shingledecker, C. N., Willis, E. R., et al. 2017, *ApJL*, **851**, L46
- McLafferty, F. W. 1959, *AnaCh*, **31**, 82
- Meinert, C., Myrgorodska, I., de Marcellus, P., et al. 2016, *Sci*, **352**, 208
- Modica, P., Martins, Z., Meinert, C., Zanda, B., & d'Hendecourt, L. L. S. 2018, *ApJ*, **865**, 41
- Monroe, A. A., & Pizzarello, S. 2011, *GeCoA*, **75**, 7585
- Mottl, M. J., Glazer, B. T., Kaiser, R. I., & Meech, K. J. 2007, *ChGC*, **67**, 253
- Muñoz Caro, G. M., & Schutte, W. A. 2003, *A&A*, **412**, 121
- Nuevo, M., Bredehöft, J. H., Meierhenrich, U. J., d'Hendecourt, L., & Thiemann, W. H.-P. 2010, *AsBio*, **10**, 245
- Nuevo, M., Cooper, G., & Sandford, S. A. 2018, *NatCo*, **9**, 5276
- Nuevo, M., Milam, S. N., Sandford, S. A., et al. 2011, *AdSpR*, **48**, 1126
- Nuevo, M., & Sandford, S. A. 2014, *ApJ*, **793**, 125
- Öberg, K. I., Garrod, R. T., Van Dishoeck, E. F., & Linnartz, H. 2009, *A&A*, **504**, 891
- Oró, J. 1961, *Natur*, **190**, 389
- Schuhmann, M., Altwegg, K., Balsiger, H., et al. 2019, *ECS*, **3**, 1854
- Shigemasa, Y., Matsuda, Y., Sakazawa, C., & Matsuura, T. 1977, *BChSJ*, **50**, 222
- Socrates, G. 2004, *Infrared and Raman Characteristic Group Frequencies* (3rd ed.; New York: Wiley)
- Sullivan, K. K., Boamah, M. D., Shulenberger, K. E., et al. 2016, *MNRAS*, **460**, 664
- Turner, A. M., Abplanalp, M. J., Chen, S. Y., et al. 2015, *PCCP*, **17**, 27281
- Yeghikyan, A. 2011, *Ap*, **54**, 87
- Zheng, W., Jewitt, D., & Kaiser, R. I. 2006, *ApJ*, **648**, 753
- Zhu, C., Frigge, R., Bergantini, A., Fortenberry, R. C., & Kaiser, R. I. 2019, *ApJ*, **881**, 156
- Zhu, C., Turner, A. M., Abplanalp, M. J., & Kaiser, R. I. 2018, *ApJS*, **234**, 15